Hysteresis in electrical parameters of saline-saturated homogeneous and layered unconsolidated sand, 200 Hz to 3 MHz

M. Kavian, E.C. Slob, and W.A. Mulder, Delft University of Technology*

SUMMARY

We measured the electric parameters for four different configurations of unconsolidated homogeneous and heterogeneous layered sands as a function of frequency, water saturation, and salinity. The ultimate objective is to determine if the effect of heterogeneities at scales much smaller than the skin depth can be captured by introducing effective frequency-dependent electrical values whose behavior can be described by simple functions. We employ the parallel-plate capacitor technique to measure complex impedance for frequencies between 200 Hz and 3 MHz. We have conducted main drainage and secondary imbibition cycles for unconsolidated sand-saline water systems at atmospheric pressure and temperatures between 21 °C and 22 °C. We found hysteresis in electric permittivity and conductivity. The hysteresis effect in the real part of the permittivity for all configurations becomes more pronounced at higher concentrations of salt except for the heterogeneous case. A description of the electric properties of a layered structure at all saturation levels by means of an effectively homogeneous medium will therefore require a dependency on both frequency and salinity of the pore fluid.

INTRODUCTION

Maxwell's equations and Ohm's law describe the diffusion of electromagnetic fields in the earth. For diffusive electromagnetic field applications, the electric conductivity is usually taken to depend only on position and not on frequency. This implies that IP effects are ignored. The introduction of a complex-valued conductivity, with an imaginary part depending on frequency, allows the inclusion of IP effects.

We want to experimentally measure the electric behavior of a layered medium as a function of water saturation and salinity for a wide range of frequencies. These dependencies are investigated for unconsolidated layered sands during imbibition, drainage, and secondary imbibition of water with different salinity levels. The key issue concerning the electrical behavior is the electric hysteresis between the drainage and the secondary imbibition processes on a continuum scale. This implies that the electric response of a medium contains information about the pore fluid distributions in a heterogeneous porous medium.

Plug et al. (2007) have measured hysteresis in the real part of electric permittivity for homogeneous sand saturated with distilled water and showed that at a fixed, optimally chosen frequency and for a given salinity the water saturation was a unique function of capillary pressure and electric permittivity. Laboratory experiments reported by Knight (1991) on sandstone show that measured values of electrical resistivity can depend on the saturation history of the sample. She found resistivity hysteresis between drainage and imbibition processes. Chelidze et al. (1999) have related this hysteric behavior to the pore-scale fluid distribution during drainage and imbibition processes. We conducted the experiment for a layered model, using sands of different grain sizes. The samples were sequentially saturated with water of three different salinity levels and the temperatures were kept between 21 °C and 22 °C. For the fully saturated case and the optimal frequency 105 kHz, the ratio of the skin depth to the layer thickness decreases with increasing salinity. This decrease is a factor 2 to 3 when we go from medium to high salinity. This result suggests that the frequency dependence of anisotropy in layered media is also a function of salinity.

EXPERIMENTAL SETUP

The sample holder, shown in Figure 1, is designed as a flat capacitor, similar to the one used by Knight and Nur (1987) or Shen et al. (1987). It has an adjustable height and consists of two parts: two porous plates acting as electrodes (SIPERM R80, porous stainless steel), each with a permeability of $3.3 \times 10^{-13}\,\mathrm{m}^2$ and a porosity of 0.33, and five PVC rings, each with a diameter of 15 cm and 3 cm height that contain the sample. To avoid leakage of water, we used sealing O-rings in between the individual PVC rings. These rings are mounted together with Teflon bolts at the top and bottom. A syringe pump (TELEDYNE ISCO pump, 1000D) was connected to the bottom of the sample holder and could be set to a constant injection or collection rate with an accuracy of 0.1 ml/min. The sample holder was put in a metallic box to shield it from external noise, see Figure 1. A precision component analyzer (Wayne-Kerr, 6640A) was used to measure the impedance amplitude, $|Z|$ [Ω], and the phase angle, ϕ [rad], as a function of the frequency. These are related to the relative effective complex permittivity, ε^*, of the sample, defined by $\varepsilon^* = \varepsilon_R - \imath\varepsilon_I$, where $\imath$ denotes the imaginary unit and the indices R and I represent the real and imaginary parts, respectively. Both ε_R and ε_I are real positive functions of frequency. We can also use the effective complex electric conductivity as $\sigma^* = \imath\omega\varepsilon_0\varepsilon^* = \sigma_R + \imath\sigma_I$, with both σ_R and σ_I real positive functions of frequency, and ε_0 is the permittivity of vacuum and ω is the angular frequency, defined by $\omega = 2\pi f$. These are related by $\sigma_R = \omega\varepsilon_0\varepsilon_I$, $\sigma_I = \omega\varepsilon_0\varepsilon_R$. We also define the effective complex electric resistivity, $\rho^* = \rho_R - \imath\rho_I$, where again both ρ_R and ρ_I are real positive functions of frequency. The resistivity is the reciprocal of electric conductivity and is given by,

$$\rho_R = \frac{\sigma_R}{\sigma_R^2+\sigma_I^2} = \frac{\varepsilon_I}{\omega\varepsilon_0(\varepsilon_R^2+\varepsilon_I^2)},\ \rho_I = \frac{\sigma_I}{\sigma_R^2+\sigma_I^2} = \frac{\varepsilon_R}{\omega\varepsilon_0(\varepsilon_R^2+\varepsilon_I^2)}.$$

We are interested in the behavior of these electric parameters as a function of frequency, water saturation, and salinity for homogeneous and flat-layered unconsolidated sand samples.

Examples

Figures 4 and 5 show the real part of relative electric permittivity as well as the real part of the conductivity versus saturation at 105 kHz in three plots, one for each salinity and in each plot the drainage and imbibition curves of coarse sand, H350(D70), fine-sand, H150(D25), and the two three layer models (B350-M150-T350 and B150-M350-T150) where B, M, and T stands for the bottom, middle, and the top layer, respectively. Each plot contains four curves for drainage and four curves for imbibition. The spectra of the permittivity and conductivity for the fully saturated case are shown in Figures 6 and 7.

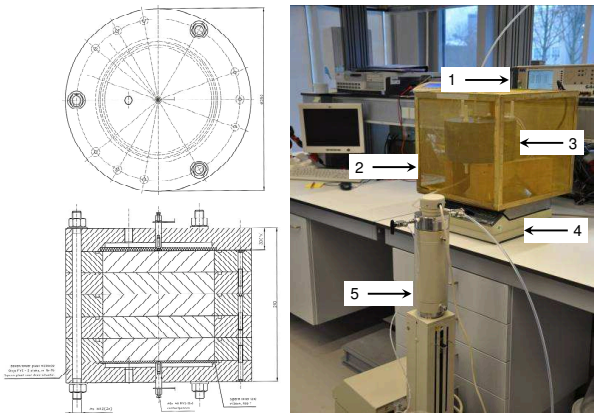

Figure 1: (Left) Schematic of the sample holder: top and front view; (right) experimental set up, 1. Component analyzer, 2. Faraday cage, 3. sample holder, 4. balance, 5. ISCO pump.

Experimental Procedure

We have used the experimental method for both the fine- and coarse-grained unconsolidated quartz sand samples and the electrical measurements run almost continuously during saturation and de-saturation cycles, for three different concentrations of salt (0.001 mol/lit, 0.01 mol/lit, and 0.1 mol/lit). The coarse and fine sands have an average grain size fraction from 350 μm to 420 μm (D70) and 150 μm to 175 μm (D25), respectively. The untreated sands, with a height of 9 cm and a diameter of 15 cm, were placed in the sample holder. We considered different combinations of a three-layer model and also two homogeneous cases with two different grain sizes of sand. These combinations are sketched in Figure 2. Four different stacks of layers were constructed and the experiment was carried out for each of them. The sample holder was vibrated for 15 minutes to reach a porosity of 0.375$\pm$0.005 and 0.395$\pm$0.005 for the coarse- and fine-grain sands, respectively. Then the sample holder was put inside the Faraday cage and filled from the bottom with water with the lowest concentration of salt (primary imbibition). During the next stage, a constant water draining flow rate of 2 ml/min was applied using the ISCO pump (main drainage process) and this process was continued until the flow stopped when the pump was no longer able to overcome the capillary pressure and could not further remove water from the sample. Then, the second imbibition process started with the pump set to water injection at the same constant flow rate as used for drainage. We determined the water saturation from the produced or injected saline water volume during drainage or imbibition, respectively, using a balance. The sample holder has a gap behind the SIPERM plates. We estimated the volume of the water that exists in this gap by looking at the change of the impedance data versus time and using the known saturation time and the saline water flow rate. For instance, in Figure 3 we have shown the impedance amplitude and phase versus time for one of the sand packs (B350-M150-T350). In each graph, we have plotted the change in impedance (phase) during saturation and drainage of the sample. The near horizontal data at the beginning and at the end of each curves illustrates the dead volume created by the gap behind the SIPERM plates.

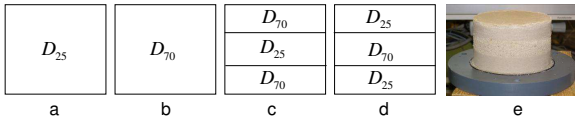

Figure 2: Four different configurations of the sand pack: (a) A homogeneous fine sand; (b) A homogeneous coarse sand; (c, d) Three layer sands with different grain size geometries; (e) Picture of the real three-layered sand sample (B150-M350-T150). The height of each layer is 3 cm, the diameter is 15 cm, and the total height is 9 cm in each configuration.

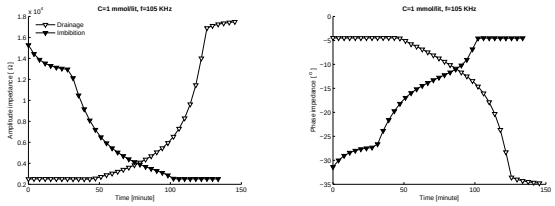

(a) (b)

Figure 3: (a) Impedance and (b) phase of data versus time in lowest salinity $C = 1$ mmol/l for the layered sand B350-M150-T350. The frequency is 105 kHz.

Data Analysis

The output of the component analyzer are the amplitude and phase of the impedance. The complex capacitance is inversely proportional to the complex impedance z^* [Ω], by $C^* = (\imath\omega z^*)^{-1}$ and $z^* = |z|e^{\imath\phi}$. The configuration is a parallel circuit for the capacitance, $C^*_{\text{total}} = C^*_{\text{sample}} + C^*_{\text{residual}}$, where C^*_{total} is the sum of the capacitance of the sample, C^*_{sample}, and the capacitance of residual contributions, C^*_{residual}, of the other parts. The capacitance of the sample is directly proportional to the sample electric permittivity given by $C^*_{\text{sample}} = \varepsilon^* \varepsilon_0 A/d$. We assume this residual capacitance to be constant, and subtract it from the total capacitance to obtain the complex relative electrical permittivity of the sample,

$$\varepsilon^*_r = \frac{d}{\imath\omega\varepsilon_0 A}\left(\frac{1}{z^*_{\text{total}}} - \frac{1}{z^*_{\text{residual}}}\right).$$

Here A [m^2] and d [m] are the cross-sectional area and the height of the sample, respectively. The value of z^*_{residual} is obtained from air measurements.

EXPERIMENTAL RESULTS AND DISCUSSION

Figure 4 shows three plots of the real part of the electric permittivity versus the water saturation at a frequency of 105 kHz, in each plot for a single salt concentration. It is clear that the permittivity changes by the change in salt concentration. For the lowest salinity, $C = 1$ mmol/l, the relative real permittivity values for all of the configurations lie between 20 and 60. Increasing the salinity by an order of magnitude leads to permittivity values between 20 and 80. Increasing the salinity by another order of magnitude causes only a big change in permittivity values of homogeneous samples H350(D70) and H150(D25), while the values that belong to the layered samples remain almost the same as for the previous concentration, except for the full saturation case. This implies that for high salinity the polarization effects are more pronounced for homogeneous samples than for layered ones. We can say that for high salinity levels the layered sample acts like a combination of capacitors, which are in series, and then the effective capacitance is less than in the homogeneous case. The drainage curves lie above the corresponding imbibition curves except for the heterogeneous case (B350-M150-T350), which contains a fine sand layer between two layers of coarse sand. We can consider this an exception, because of more absorption of water by the grains, since this configuration was under test longer than the other configurations. The drainage curves for the other heterogeneous case (B150-M350-T150), where the layer of coarse sand is inserted between two layers of fine sand, run almost in parallel and lie above the corresponding imbibition curves. The non-monotonic behavior in permittivity is seen for all experiments. It shows a maximum and has a smooth appearance. The maximum lies between 0.87 and 0.92, depending on salinity. The behavior of the real part of the electric conductivity versus saturation, shown in Figure 5, is completely different from that of the permittivity. In Figure 5(a), obtained at the lowest salinity with a concentration of $C = 1$ mmol/l, the drainage curves lie above the corresponding imbibition curves except for the homogeneous fine sand (H150). All the curves follow a monotonic behavior except for saturations higher than 0.95. Increasing salinity by an order of magnitude brings the imbibition curve of H350 above the corresponding drainage curve. Also, the curves become more parallel to each other. Increasing the salinity by another order of magnitude does not cause any displacement between drainage and corresponding imbibition curves. As shown in Figure 5(c), at low and full saturation levels the conductivity values of drainage coincide with the values measured for the corresponding imbibition processes only for those two configurations that consist of homogeneous coarse sand H350(D70) and the layered sample B350-M150-T350. The most commonly used formula for describing the variation of electric conductivity with saturation S_w introduced by Archie (1942), in which the electric conductivity is proportional to S_w^n, where n is referred to as the saturation exponent. Figure 5 apparently shows that the variation in electric conductivity with S_w and salinity is more complicated than can be described by Archie's relationship. The complexity increases when we include the frequency dependency of electric conductivity into account. Figures 6 and 7 show the frequency response of the relative real part of permittivity and real part of electric conductivity in the frequency range between 2.1 kHz and 3 MHz for fully saturated level. As indicated in Figure 6 at high saturations ($S_w = 1$), the permittivity of the samples show significant dispersion with permittivity decreasing with increasing frequency. This situation for the real electric conductivity, however, shows little dependence on frequency until frequencies above approximately 1 MHz. This weak frequency dependence shifted to higher frequencies when we go to higher salinity as we can see in Figure 7(c).

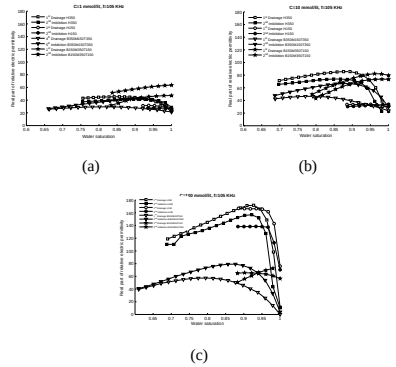

(a) (b)

(c)

Figure 4: Hysteresis in the real part of electric permittivity for four different combinations of unconsolidated sand in three different salt concentrations; (a) $C = 1$ mmol/l, (b) $C = 10$ mmol/l, and (c) $C = 100$ mmol/l. The frequency is 105 kHz.

CONCLUSION

The possibility of replacing a layered structure by an effectively homogeneous medium to define its electric properties has been shown to depend on frequency and salinity of the pore fluid. The reasons for the observed permittivity hysteresis can be found in the distribution of the water and gas phase **?** as well as in the change in interfacial area during saturation and de-saturation processes. Plug et al. (2007) has found a small hysteresis in permittivity for 3 MHz during drainage and imbibition and related that to the re-distribution of the water and gas phase. We found experimentally that the hysteresis effect of permittivity becomes more pronounced for lower frequencies (i.e. 105 kHz), where the change in interfacial area can be the dominant reason. The hysteresis effect is a function of salinity and the kind of samples under the test. Also, repeating the drainage and imbibition cycles for 4^{th} and 5^{th} times, respectively, moves the permittivity imbibition curve above the corresponding drainage curve. This effect is not seen in conductivity hysteresis as shown in Figure 5. This implies that the dependence of geophysical data on saturation history should be considered.

ACKNOWLEDGMENTS

We thank H.K.J. Heller and F.C. Riem Vis for technical support and Delft Earth and Shell for funding the project.

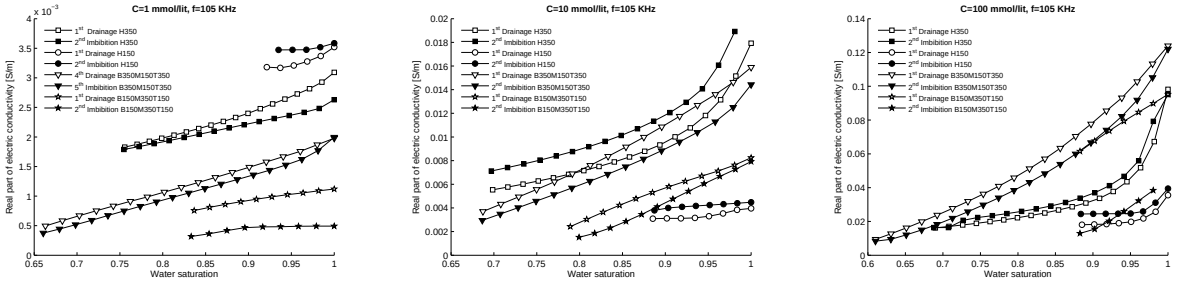

(a) (b) (c)

Figure 5: Hysteresis in real part of the electric conductivity for four different combinations of unconsolidated sand in three different salt concentrations; (a) $C = 1\,\text{mmol/l}$, (b) $C = 10\,\text{mmol/l}$, and (c) $C = 100\,\text{mmol/l}$. The frequency is 105 kHz.

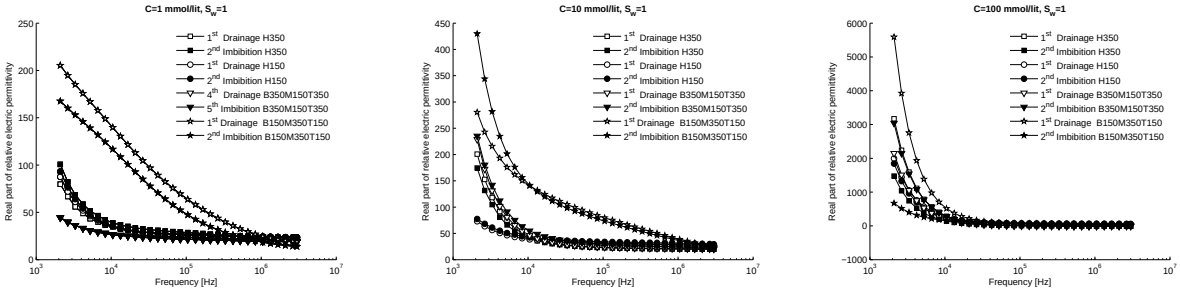

(a) (b) (c)

Figure 6: Real part of relative electric permittivity versus frequency for four different combinations of unconsolidated sand in three different salt concentrations; (a) $C = 1\,\text{mmol/l}$, (b) $C = 10\,\text{mmol/l}$, and (c) $C = 100\,\text{mmol/l}$. The saturation level is 1.

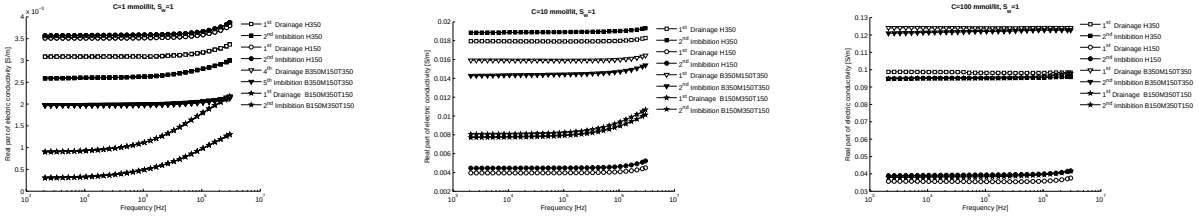

(a) (b) (c)

Figure 7: Real part of electric conductivity versus frequency for four different combinations of unconsolidated sand in three different salt concentrations; (a) $C = 1\,\text{mmol/l}$, (b) $C = 10\,\text{mmol/l}$, and (c) $C = 100\,\text{mmol/l}$. The saturation level is 1.

EDITED REFERENCES

Note: This reference list is a copy-edited version of the reference list submitted by the author. Reference lists for the 2009 SEG Technical Program Expanded Abstracts have been copy edited so that references provided with the online metadata for each paper will achieve a high degree of linking to cited sources that appear on the Web.

REFERENCES

Archie, G., 1942, The electrical resistivity log as an aid in determining some reservoir characteristic: American Institute of Mining, Metallurgical and Petroleum Engineering, **146**, 54–67.

Chelidze, T., Y. Gueguen, and C. Ruffet, 1999, Electrical spectroscopy of porous rocks: A review – II. Experimental results and interpretation: Geophysical Journal International, **137**, 16–34.

Knight, R., 1991, Hysteresis in the electrical resistivity of partially saturated sandstones: Geophysics, **56**, 2139–2147.

Knight, R. and A. Nur, 1987, The dielectric constant of sandstones, 60 kHz to 4 MHz: Geophysics, **52**, 644–654.

Plug, W., E. Slob, J. Bruining, and L. M. Tirado, 2007, Simultaneous measurement of hysteresis in capillary pressure and electric permittivity for multiphase flow through porous media: Geophysics, **72**, no. 3, A41–A45.

Shen, L., H. Marouni, Y. Zhang, and X. Shi, 1987, Analysis of the parallel-disk sample holder for dielectric permittivity measurement: IEEE Transactions on Geoscience and Remote Sensing, 25, 534–540.